

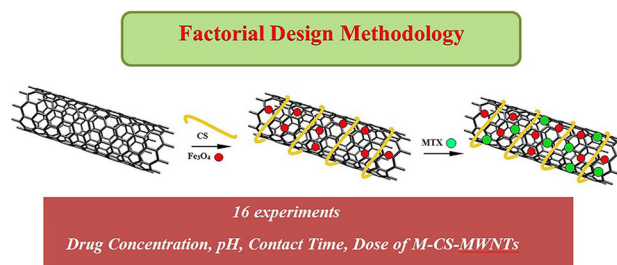
Kinetic and thermodynamic studies of methotrexate adsorption on chitosan-modified magnetic multi-walled carbon nanotubes

Bahman Vasheghani Farahani¹ · Nasrin Javadi¹

Received: 9 January 2016 / Accepted: 3 April 2016 / Published online: 25 April 2016
© Springer-Verlag Wien 2016

Abstract A new type of drug delivery system involved chitosan (CS)-modified magnetic multi-walled carbon nanotubes (M-CS-MWNTs) was synthesized. Prepared M-CS-MWNTs was characterized by Fourier transform infrared spectroscopy, scanning electron microscope, thermogravimetric analysis, X-ray diffraction, and CHN techniques. The nanocarrier was used for controllable loading and release of anticancer drug methotrexate. The full factorial design methodology was employed to obtain the optimum conditions for time, dose of adsorbent, initial methotrexate concentration, and pH of preparative media on the drug loading efficiency, by using Minitab 16 and Design Expert 7.1.6 software. The maximum loading (89 %) was achieved under optimized condition (pH: 7.0, time: 35 min, methotrexate concentration: 20 mg dm⁻³, and M-CS-MWNTs dosage: 0.20 g dm⁻³). The adsorption isotherm and other properties including kinetics and thermodynamics were studied. Pseudo-second order shows the best fitting of methotrexate adsorption. The thermodynamic studies showed that the adsorption of methotrexate on nanocarrier is spontaneous and exothermic in nature.

Graphical abstract



Keywords Drug research · Nanostructures · Thermodynamics · Isotherm · Full factorial design

Introduction

Chemotherapy is often used to treat a disease, such as cancer by powerful chemicals drugs to kill cancer cells whilst minimizing side effects to healthy tissue and maximum treatment efficacy [1]. However, conventional anticancer drugs often have some unexpected limitations such as limited solubility, poor nonselective biodistribution, and tissue damage; therefore, they are far from ideal. To overcome these problems, nano-sized delivery vehicles have been employed to improve the therapeutic and pharmacological properties of the anticancer drugs by controlling release rates and targeted delivery process.

Many different types of drug delivery systems are currently available. Among the currently available delivery vehicles such as polymeric nanoparticles [2–4], liposomes [5–7], and inorganic nanoparticles [8], CNTs have emerged

Electronic supplementary material The online version of this article (doi:10.1007/s00706-016-1753-3) contains supplementary material, which is available to authorized users.

✉ Bahman Vasheghani Farahani
bvasheghanif@gmail.com

¹ Department of Chemistry, Faculty of Science, Imam Khomeini International University, PO Box 288, Qazvin 34149, Islamic Republic of Iran

as a new alternative and efficient tool for transporting and translocating therapeutic molecules due to their significant advantages including higher accumulation in tumor tissues as compared to normal tissues, high aspect ratios and surface areas, cell membrane penetrability, high capacities for drug loading, and prolonged circulating time [9–12].

Large numbers of CNTs-based drug delivery systems (DDSs) with chemotherapy effects have been designed and evaluated at the cellular level [13–18]. CNTs are hydrophobic in nature and thus insoluble in water, which limits their application in biomedical and medicinal chemistry. In the recent years, covalent and non-covalent functionalization of carbon nanotubes with polymers has been of significant interest [19]. Modification of CNTs with biopolymers has attracted significant interest due to their hydrophilicity, dispersion in aqueous solution, and excellent adsorption properties [20–24]. The strategy of polymer functionalization not only provides an effective approach to improve the solubility and biocompatibility of carbon nanotubes for biotechnological applications, but also offers a practical protocol for the preparation of polymeric nanocomposite as potential sorbent in pharmaceutical sciences.

Among those biopolymers used for modification of CNTs, chitosan is an excellent kind of modifier. Chitosan is well known as nontoxic and biologically degradable [25, 26] material in pharmaceutical sciences due to its high hydrophilicity, flexible polymer structure, and large number of functional groups (acetamido, primary amino and/or hydroxyl groups) on the backbone [27, 28]. Some studies have demonstrated that the dispersion of CNTs could be dramatically improved using chitosan possibly due to a higher surface coverage of the CNTs [24, 29].

Methotrexate (MTX) is a well-known and potent antifolate, used also to treat autoimmune diseases. However, MTX suffers from poor bioavailability, low cellular uptake, and toxic systemic side effects [30]. Combining MTX with functionalized CNTs has the potential to raise the bioavailability of MTX and diminish its undesirable adverse effects by delivering MTX specifically to tumor cells with additional targeting molecules [31]. To further augment the efficacy of CNT-based drug delivery system (DDS), magnetic nanoparticles (MNPs) have received extensive attention in biomedical communities due to their potentials in medical applications [32]. CNTs can also enter cells under the application of an external magnetic field, which provides an active magnetic targeting mechanism [33].

Although several studies have been reported on the effects of *in vivo* or *in vitro* antitumor activity and tumor targeting of drug–CNTs complex based on the adsorption, but very little is known about the adsorption behavior of anticancer drug on CNTs. To facilitate the development of the CNT-based drug delivery systems, thorough studies of

the adsorption and desorption of drugs on CNTs are absolutely necessary. In this work, we present our attempt to construct a type of chitosan (CS) modified magnetic multi-walled carbon nanotubes (MWNTs) for controllable loading/release of anti-cancer agent methotrexate (MTX) from aqueous solution. In fact, CS was non-covalently wrapped around MWNTs, imparting water solubility and biocompatibility to the nanotubes. Fe₃O₄ nanoparticles were also bounded to the outer MWNTs layer to realize selective killing of tumor cells. The final product was (M-CS-MWNTs).

In this study, mainly focused on the effect of time, initial drug concentration, M-CS-MWNTs dosage, pH, the adsorption kinetic, equilibrium and thermodynamic parameters at various temperatures and concentrations. To optimize the independent variables, (i.e., pH, contact time, drug concentration, and adsorbent dosage) on dependent variables, (i.e., entrapment efficiency), were investigated by a two-level, four-factor, full factorial experimental design with Minitab 16 and Design Expert 7.1.6 softwares.

Results and discussion

Nanocarrier characterization

To know the surface functional groups, morphology, and structure of the adsorbent, the following studies were conducted.

FT-IR analysis

Fourier transform infrared (FT-IR) spectra of (a) Fe₃O₄, (b) MWNTs, (c) MWNTs-COOH, (d) CS, and (e) M-CS-MWNTs are shown in Fig. 1. In Fig. 1a, the characteristic peak at 624 cm⁻¹ is attributed to the Fe–O stretching vibration. The peak observed at about 3444 cm⁻¹ shows the presence of hydroxyl group, probably due to the presence of moisture in the air. The peaks are observed in MWNTs spectra at 1153, 1639, and 3489 cm⁻¹ wavelength are related to C–O, C=C, and O–H bonds, respectively (cf. Fig. 1b). It should be mentioned that the peaks observed for C–O and O–H bonds are related to low percent of hydroxyl group on nanotubes surface. The peaks observed in functionalized MWNTs-COOH spectra at 1166, 1703 cm⁻¹ are related to C–O and C=O, respectively (Fig. 1c). The wide peak, which is appeared in the region of 3448.56 cm⁻¹ assigned to O–H (carboxylic acid) group. Observed peaks at 2860.26 and 2924.39 cm⁻¹ are due to C–H stretching bonds. In fact, increasing intensity and width of O–H peaks are due to functionalizing of nanotubes by HNO₃. On comparing Fig. 1b, c, it can be said

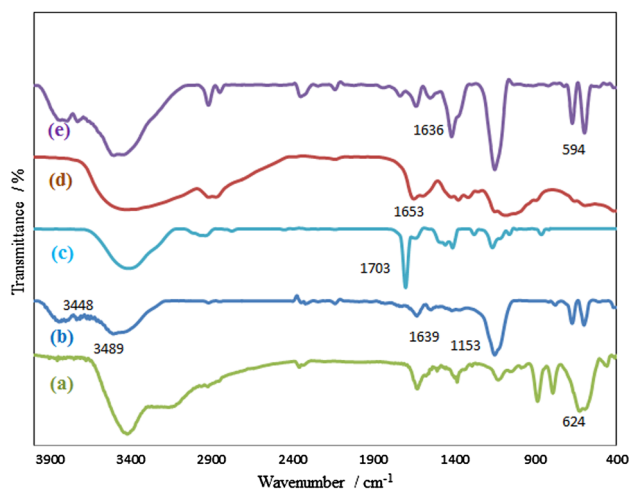


Fig. 1 FT-IR spectra of *a* Fe₃O₄, *b* MWNTs, *c* MWNTs-COOH, *d* CS, and *e* M-CS-MWNTs

that MWNTs were successfully oxidized by HNO₃. In Fig. 1d, the characteristic peaks at 1084, 1653, and 3426 cm⁻¹ are related to the stretching vibration of C–O, N–H, and O–H bonds, respectively. The shift in the NH stretching peak from 1653 cm⁻¹ to lower wave number (1636 cm⁻¹) in the M-CS-MWNTs (cf. Fig. 1e) suggested that the MWNTs is well coated with chitosan. In the spectrum of M-CS-MWNTs, the characteristic peak at 594 cm⁻¹ indicates the displacement of Fe₃O₄ spectrum to lower wave number due to Fe–O bond. This reveals that a nanocarrier has magnetic properties.

Thermal analysis

The thermal behavior of MWNTs, CS, and M-CS-MWNTs are presented in Fig. 2. Due to the high thermal stability of MWNTs, thermal gravimetric analysis technique (TGA) has been widely used to quantify the MWNTs' degree of functionalization [34]. Therefore, this technique has been used for quantitative analysis of polymers linked to

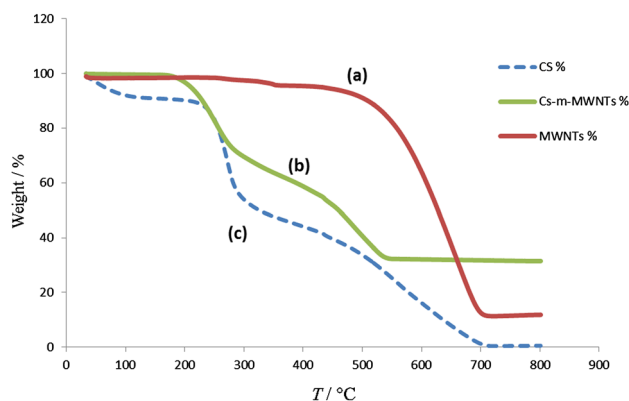


Fig. 2 TGA of *a* MWNTs, *b* M-CS-MWNTs, and *c* CS

nanotubes. As can be seen from Fig. 2, two weight losses are shown in M-CS-MWNTs. Obvious weight loss is observed for the M-CS-MWNTs when the temperature became higher than 200 °C, due to the pyrolysis of the deposited chitosan.

XRD analysis

The XRD pattern of M-CS-MWNTs is shown in Fig. 3. The XRD spectra show the presence of peaks corresponding to both chitosan and carbon nanotube [35, 36]. There are also six characteristic peaks for Fe₃O₄ at $2\theta = 30.1^\circ, 35.5^\circ, 43.3^\circ, 53.4^\circ, 57.2^\circ,$ and 62.5° where all diffraction peaks can be well indexed to the (2 2 0), (3 1 1), (4 0 0), (4 2 2), (5 1 1), and (4 4 0) planes (JCPDS No. 19-0629), indicating that both Fe₃O₄ and M-CS-MWNTs exhibited typical Fe₃O₄ cubic structure. The results obtained from XRD studies also clearly show the formation of nanocarrier.

Elemental analysis (CHN)

Elemental analysis was applied to determine the nitrogen content of the nanocarrier (Table 1). In comparison with unmodified MWNTs, a significant increase in nitrogen content of M-CS-MWNTs approves the chitosan coated on the surface of MWNTs. The elemental analysis results revealed that for 1.0 g MWNTs, 3.76 mmol chitosan grafted to it.

Raman analysis

Figure 4 shows the Raman spectra of pristine MWNTs and M-CS-MWNTs. The Raman spectra of pristine MWNTs show two characteristic peaks (D and G bands). One at the Raman shift of 1309 cm⁻¹ named D band, which is associated with the defects present in the graphitic structure to the disordered graphitic structure of MWNTs. The other peak at the Raman shift of 1578 cm⁻¹ named G-band,

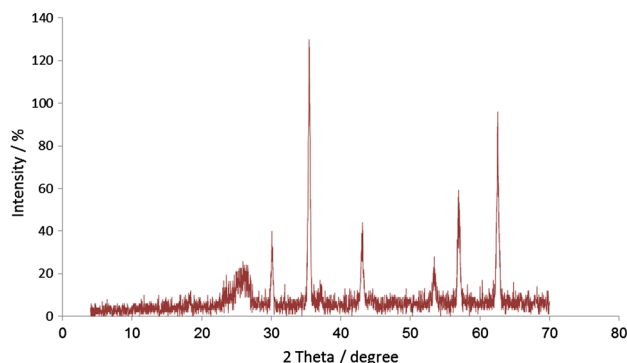
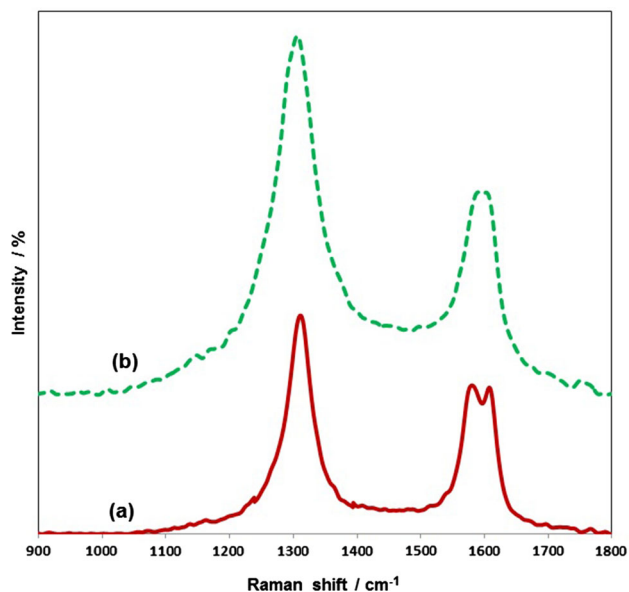


Fig. 3 XRD patterns of M-CS-MWNTs

Table 1 Elemental analysis of MWNTs, MWNTs-COOH, M-CS-MWNTs

Name	C (%)	H (%)	N (%)
MWNTs	97.2	0.390	0.0
MWNTs-COOH	96.40	0.420	0.0
M-CS-MWNTs	89.2	3.40	1.65

**Fig. 4** Raman spectra of *a* MWNTs, *b* M-CS-MWNTs

which assigned to the C=C bond in the graphitic plane. The intensity relation between the two bands (I_D/I_G) is the most widely used tool to evaluate the grafting of carbon nanotubes [37, 38]. When the MWNTs surfaces coated by CS and Fe_3O_4 , it was found that the Raman D band intensity increased. Thus, the intensity ratio of D band to G band (I_D/I_G) can be used for evaluation of graphitic structure of CNTs.

SEM images

SEM images for (a) MWNTs-COOH, (b) Fe_3O_4 , (c) CS, and (d) M-CS-MWNTs are given in Fig. 5. The images show a clear morphology of these compounds. Image of MWNTs-COOH reveal a smooth surface with curled and entangled tubes (Fig. 5a). Whereas the surfaces of carbon nanotubes in M-CS-MWNTs after the deposition of chitosan and Fe_3O_4 nanoparticles, changed significantly and the surfaces of carbon nanotubes in M-CS-MWNTs were rough and existed some clusters attached to them (Fig. 5d). This reveals that chitosan and Fe_3O_4 has been coated on the surface of MWNTs.

Experimental design

The factorial design method can be used to achieve the best experimental conditions to increase the reaction efficiency. The advantage of using this method is to reduce experiment costs and also to save time. After applying optimum conditions to adsorption of MTX on M-CS-MWNTs system, the obtained experimental data were best fitted in this model.

The Minitab 16 software was used to find the best condition leading to the highest drug loading efficiency. Equation (1) demonstrates the relationship between the variables as follows:

$$R\% = 65.55 + 9.38A + 5.55B + 0.794C + 3.75D + 0.327AC - 2.42AD - 0.037AB - 0.283CD - 3.85BC - 1.31BD + 1.27ACD - 3.61ABC - 3.32ABD - 0.93BCD - 0.88ABCD \quad (1)$$

where A, B, C, and D parameters are explained in Table 2. More information of the experimental design and analysis of the variance (ANOVA) of the model has presented in the Supplementary Material.

In addition to statistical tests, the adequacy of the model was also evaluated through the difference between the observed and predicted values. A satisfactory correlation between the observed and predicted values of MTX adsorption efficiency is shown in Fig. 6. The model predicted the optimal values of the four variables pH: 7.0, time: 35 min, initial drug concentration: 20 mg dm^{-3} , and adsorbent dosage: 0.20 g dm^{-3} corresponding to maximum loading = 89 %.

The Pareto chart

The relative importance of the main effects and their interactions was also observed on the Pareto chart. According to Fig. 7, the sequence of very important main factors and their interactions may be expressed as: $A > B > BC > D > ABC > ABD > AD$, following a decreasing influence on the adsorbed amount of methotrexate. The last three factors in the sequence, AC, CD, and AB having their *t* values under the Bonferroni limit are marked non-significant. The interactions BD, ACD, BCD, and ABCD may be considered as moderately important, while the single factor C is slightly significant. Three interactions CD, AC, and AB are considered non-important factors and insignificant.

Kinetic studies

Various kinetic models such as pseudo-first order, pseudo-second order, Elovich, and intra-particle diffusion models

Fig. 5 SEM images of **a** MWNTs-COOH, **b** Fe₃O₄, **c** CS, and **d** M-CS-MWNTs

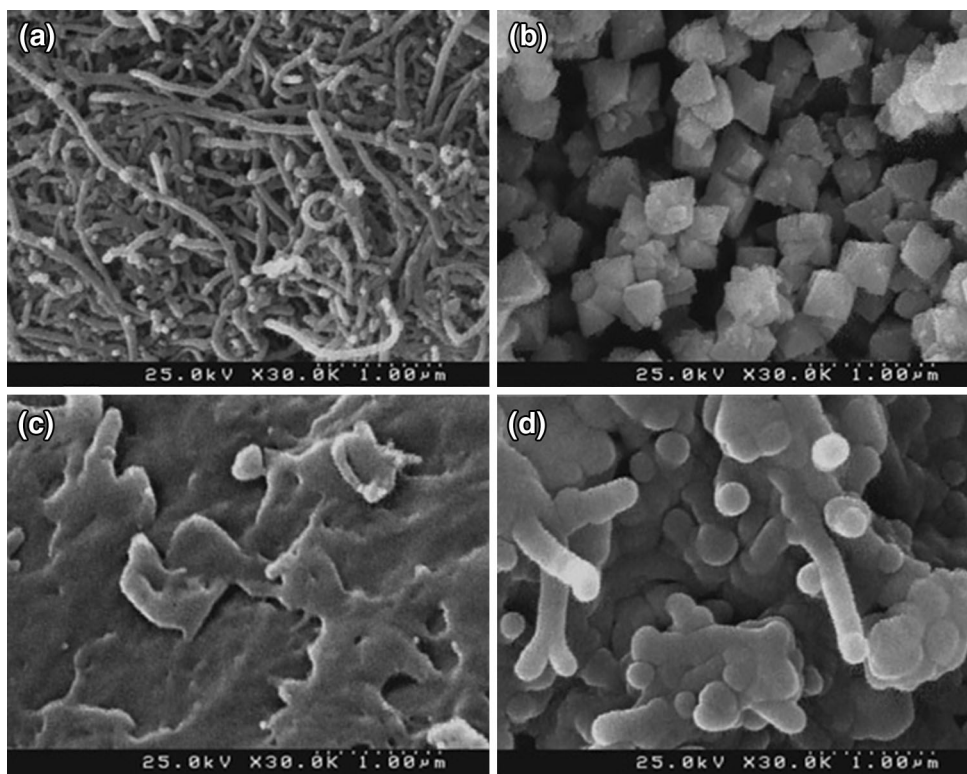


Table 2 Experimental ranges and levels of the factors used in the factorial design

Independent variable	Coded symbol	Level	
		-1	1
Solution pH	A	3.0	7.0
Time/min	B	3	35
Adsorbent dosage/g dm ⁻³	C	0.2	1.2
Drug concentration/mg dm ⁻³	D	20	50

are used to study the kinetic adsorption of the MTX on the nanocarrier [39–41].

A simple kinetic model given by Lagergren is the pseudo-first-order relation:

$$q_t = q_e(1 - e^{-k_1t}) \quad \text{Pseudo-first order} \quad (2)$$

The experimental data were also tested by the pseudo-second-order kinetic model which is shown as Eq. (3):

$$q_t = \frac{k_2q_e^2t}{1 + k_2q_e t} \quad \text{Pseudo-second order} \quad (3)$$

where q_t (mg g⁻¹) and q_e (mg g⁻¹) are the adsorption capacity at any time t (min) and the equilibrium adsorption capacity, respectively; k_1 and k_2 are the pseudo-first-order (min⁻¹) and the pseudo-second-order rate constant (g mg⁻¹ min⁻¹), respectively.

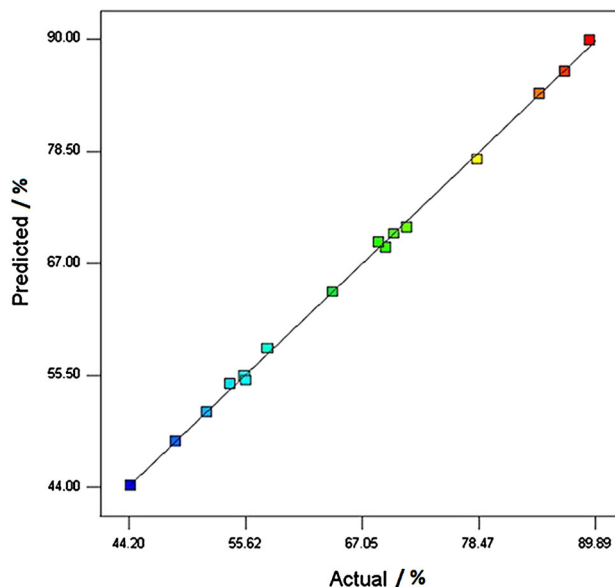


Fig. 6 Correlation between the experimental and predicted values

The Elovich model is studied by the following equation:

$$q_t = \frac{1}{\beta} \ln \alpha \beta + \frac{1}{\beta} \ln t \quad \text{Elovich model} \quad (4)$$

where α is the initial adsorption rate (mg g⁻¹ min⁻¹) and β is the desorption constant (g mg⁻¹). The intra-particle

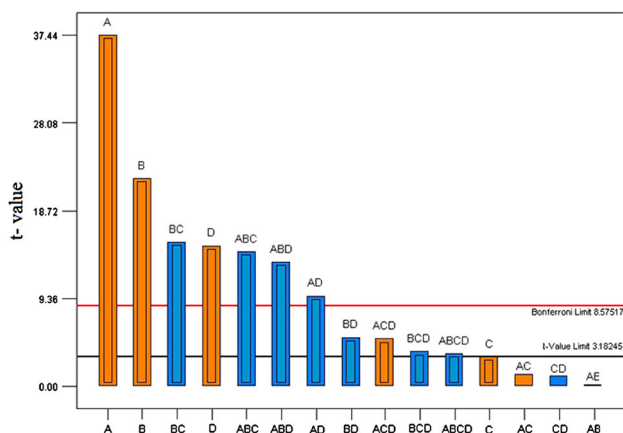


Fig. 7 Pareto chart of effects

diffusion model is widely used to predict the rate controlling step. The rate constant of intra-particle diffusion (k_i) at stage i is determined using the following equation:

$$q_t = k_i t^{1/2} + C_i \quad \text{Intraparticle diffusion model} \quad (5)$$

where k_i is the rate constant at stage i and C_i is related to the thickness of the boundary layer of intra-particle diffusion model.

Since non-linear method is an appropriate model to predict the optimum sorption kinetics [42, 43], therefore the experimental data were fitted to the kinetics models by non-linear regression, trial and error method using Solver add-In in Microsoft Excel. The corresponding kinetic parameters are summarized in Table 3. The validity of each kinetic model was checked by regression index R^2 and residual sum of squares (RSS). The experimental data and predicted kinetics models shown in Fig. 8.

Curves in Fig. 8 reveal that MTX adsorption on M-CS-MWNTs easily take place, as 90 % of the adsorption achieved within initial 7 min. On comparing the R^2 and RSS for the different models (Table 3), it can be said that the pseudo-second order is the best model as it has the

highest regression coefficients values (R^2) and the lowest RSS. Its equilibrium sorption capacity is 19.2 mg g^{-1} which is very close to experimental value. The better fit of the pseudo-second-order model, therefore, indicates that the adsorption depends on the adsorbate as well as the adsorbent and involves chemisorption process (electrostatic interaction, hydrogen bonding, and π - π stacking interaction) in addition to physisorption.

Isothermal studies of the adsorption

The isotherm study was carried out by varying initial MTX concentration from 20 to 90 mg dm^{-3} at temperature range 293–310 K (Fig. 9). Two conventional adsorption isotherms, Freundlich and Langmuir models, were employed to describe the MTX adsorption equilibrium [44].

The Langmuir isotherm is a theoretical model derived base on the assumptions that adsorption is monolayer, homogeneous and without lateral interactions between adsorbing species and is expressed as

$$Q_e = \frac{q_{\max} C_e}{1 + K_L C_e} \quad (6)$$

where C_e is equilibrium solution concentration (mg dm^{-3}), Q_e is the equilibrium adsorption capacity of nanocarrier (mg g^{-1}), q_{\max} is the maximum adsorption capacity, and K_L is the Langmuir constant related to affinity of the binding sites.

Freundlich model is an empirical equation based on adsorption on a heterogeneous surface or surfaces supporting sites of varied affinities. It is assumed that the stronger binding sites are occupied first and that the binding strength decreases with the increasing degree of site occupation. The isotherm is expressed as

$$q_e = k_F C_e^{1/n} \quad (7)$$

where $1/n$ is an empirical parameter related to adsorption intensity and k_F is a Freundlich constant related to adsorption capacity ($\text{dm}^3 \text{ g}^{-1}$). The magnitude of the exponent n gives an indication on the favorability of

Table 3 Kinetic parameters for MTX adsorption on M-CS-MWNTs by various kinetic models

Kinetic model	Parameters	Values	Kinetic model	Parameters	Values
Pseudo-first order	$q_e/\text{mg g}^{-1}$	17.4	Elovich	$\alpha/\text{mg g}^{-1} \text{ min}^{-1}$	56.0
	k_1/min^{-1}	0.302		$\beta/\text{g mg}^{-1}$	0.351
	R^{2a}	0.991		R^2	0.993
	RSS ^b	2.55		RSS	1.99
Pseudo-second order	$q_e/\text{mg g}^{-1}$	19.2	Intra-particle diffusion	$C_i/\text{mg g}^{-1}$	9.64
	$k_2/\text{g mg}^{-1} \text{ min}^{-1}$	0.023		$k_i/\text{mg g}^{-1} \text{ min}^{1/2}$	1.59
	R^2	0.999		R^2	0.997
	RSS	0.310		RSS	6.05

^{a,b} R is correlation coefficient and RSS is residual sum of squares

Fig. 8 Adsorption kinetics of MTX on M-CS-MWNTs: **a** pseudo-first order; **b** pseudo-second order; **c** Elovich, and **d** intra-particle diffusion models

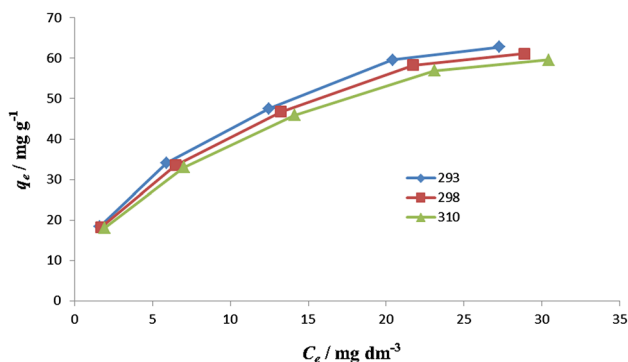
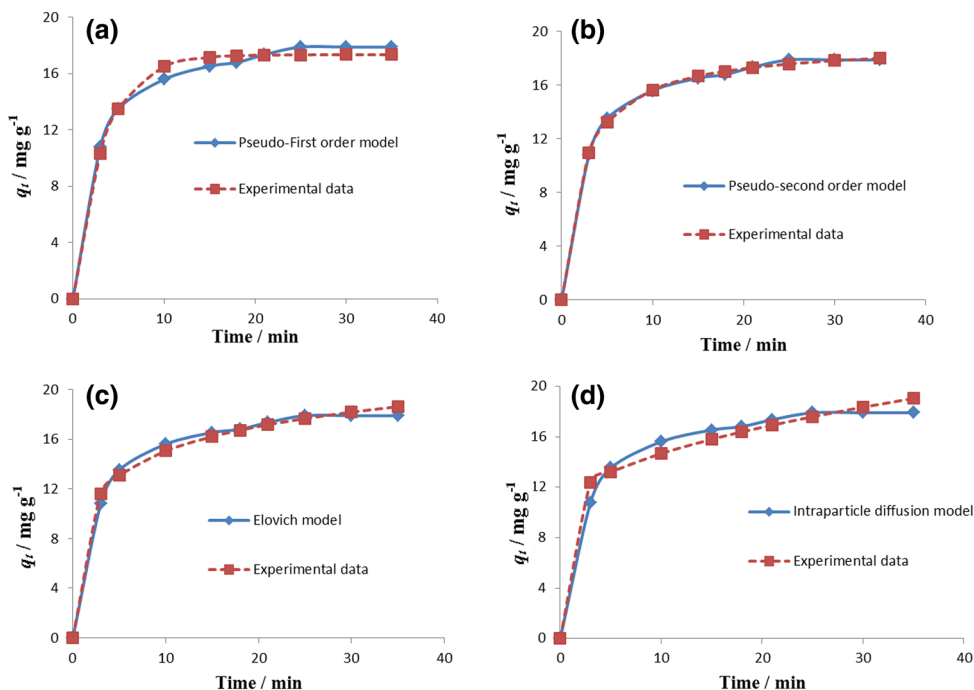


Fig. 9 Effect of temperature on MTX adsorption (C_0 : 20, 40, 60, 80, and 90 mg dm^{-3} , $m_{(\text{M-CS-MWNTs})}$: 0.20 g dm^{-3} , pH: 7.0, time: 35 min)

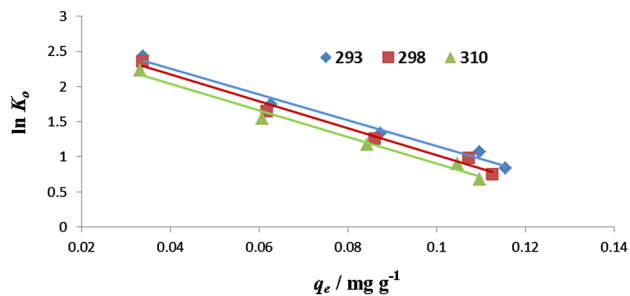


Fig. 10 Plots of $\ln(q_e/C_e)$ vs. q_e for MTX adsorbed on M-CS-MWNTs

adsorption. It is generally stated that values of n in the range 2–10 represent good, 1–2 moderately difficult, and less than 1 poor adsorption characteristics. The isotherm

constants and determination coefficients are summarized in Table 4.

The Freundlich isotherm provided much better fit to the equilibrium data compared with the Langmuir isotherm

Table 4 Isotherm parameters for the adsorption of MTX on M-CS-MWNTs

Temperature/ $^{\circ}\text{C}$	Langmuir isotherm model			Freundlich isotherm model		
	$q_{\text{max}}/\text{dm}^3 \text{ g}^{-1}$	$K_L/\text{dm}^3 \text{ mg}$	R^2	$K_F/\text{dm}^3 \text{ g}^{-1}$	n	R^2
288	11.1	0.141	0.983	16.0	2.36	0.991
298	10.2	0.134	0.982	15.4	2.38	0.991
310	9.28	0.124	0.984	14.5	2.36	0.990

R^2 correlation coefficient, q_{max} maximum adsorption capacity, K_L Langmuir constant related to affinity of the binding sites, K_F and n are Freundlich constants

Table 5 Thermodynamic parameters for MTX adsorption on M-CS-MWNTs

Thermodynamic parameters	(K_0)	($\Delta G^0/\text{kJ mol}^{-1}$)	($\Delta H^0/\text{kJ mol}^{-1}$)	($\Delta S^0/\text{J K}^{-1}\text{mol}^{-1}$)
293	19.9	-7.29	-8.43	-3.92
298	18.7	-7.26		
310	16.4	-7.22		

based on the higher R^2 (0.990–0.991) values. This result may be due to the heterogeneous distribution of active sites on the edge and two sides of the nanocarrier. The results show that the values of the Freundlich exponent n were greater than 2, which confirm that the adsorption for the MTX is favorable.

Thermodynamic studies

The nature of adsorption can be characterized by calculating the thermodynamic parameters such as enthalpy change (ΔH^0), entropy change ΔS^0 , and Gibbs free energy change (ΔG^0) using equilibrium adsorption data obtained at various temperatures. The following Eqs. (8–10) were used to estimate the thermodynamic parameters [45]:

$$\ln K_0(T_3) - \ln K_0(T_1) = \frac{-\Delta H^0}{R} \left(\frac{1}{T_3} - \frac{1}{T_1} \right) \quad (8)$$

$$\Delta S^0 = - \frac{\Delta G^0 - \Delta H^0}{T} \quad (9)$$

$$\Delta G^0 = -RT \ln K_0 \quad (10)$$

where (ΔH^0) (kJ mol^{-1}), (ΔG^0) (kJ mol^{-1}), and (ΔS^0) ($\text{J mol}^{-1} \text{K}^{-1}$) are changes of free energy, enthalpy, and entropy, respectively; R is the universal gas constant ($8.314 \text{ J mol}^{-1} \text{ K}^{-1}$); T is the absolute temperature (K); (K_0) is ratio of concentration of MTX on adsorbent at equilibrium (q_e) to the remaining concentration of the MTX in solution at equilibrium (C_e). K_0 can be obtained from the intercept of $\ln(q_e/C_e)$ vs. q_e plot (Fig. 10). As listed in Table 5, the negative values of ΔG^0 and ΔH^0 reveal that the adsorption process is spontaneous and exothermic. Also, the negative value of ΔS^0 indicates decreased randomness at the adsorbent/solution interface during the adsorption of MTX on nanocarrier.

Conclusion

In this research work, the M-CS-MWNTs adsorbent was prepared and characterized by using several methods. The results showed that the nanocarrier was successfully synthesized. The performance of M-CS-MWNTs as a carrier for controlled release of MTX was investigated. For this purpose, the drug loading and release behavior of the

modified MWNTs were studied. The effect of pH, time, initial drug concentration and adsorbent dosage on the adsorption of the MTX in the nanocarrier was investigated by full factorial experimental designs. The results from full factorial design showed that the pH has the most significant effect on the adsorption and also adsorbent dosage has the least effect on it. This model showed satisfactory correlation between the observed and predicted values of MTX adsorption efficiency. Under optimal conditions, 89 % of MTX adsorption was achieved. The kinetic and isothermal studies were considered by non-linear regression method. The kinetics process can be successfully described and well fitted to the pseudo-second-order kinetic model indicating the possible involvement of chemisorption. The adsorption isotherms were best explained by the Freundlich model, which indicate heterogeneous surface where the stronger binding sites are occupied first and the binding strength decreases with the increasing degree of site occupation. The negative values of ΔG^0 indicate the spontaneous nature of MTX adsorption on the adsorbent and negative values of ΔS^0 confirms a decrease of randomness of the adsorbent/solution. The negative value of ΔH^0 reveals the exothermic nature of the adsorption and in this case electrostatic interactions are dominant.

Experimental

Reagents and materials

Multi-walled carbon nanotubes (outer diameter 5–15 nm, length about 30 μm) was purchased from US Research Nanomaterials, Co., Ltd. Chitosan (CS) with approximate molecular weight 5000 and 85 % degree of distillation was received from Novinshimiar. Methotrexate, used as a model anticancer drug was obtained from the Sigma Aldrich Co. Fe_3O_4 nanoparticle (15–20 nm) was received from US Research Nanomaterials, Co., Ltd. The other reagents of analytical grade were purchased from Merck Co. Ltd and they were used without further treatment.

Instrumentation

Fourier transform infrared (FT-IR) spectra were recorded by using the FT-IR spectrophotometer (Baker Tensor 27

FT-IR). Thermal gravimetric analyses (TGA) were carried out on a differential scanning calorimeter (Perkin Elmer-USA) with a heating rate of $10\text{ }^{\circ}\text{C min}^{-1}$ under nitrogen environment. Scanning electron microscope (SEM) model AIS 2100 from Soren technology is used to obtain morphological information of the surface. X-ray diffraction (XRD) measurements were performed on powdered samples in a Bruker Advance D8 X-ray diffractometer. The voltage and current used were 40 kV and 30 mA, respectively, and XRD patterns were obtained in the 2θ range of 10° – 70° at $5^{\circ}\text{ min}^{-1}$ scanning speeds. Carbon, hydrogen and nitrogen contents of the samples were determined (CHN techniques) using a Vario EL III elemental analyzer. The concentrations of the MTX solution were determined with a UV–Vis spectrometer (Cam Spec model M350). Raman scattering spectra obtained at room temperature using a Horiba JobinYvon high-resolution Lab Ram Raman microscope system equipped with a charge-coupled detector, confocal microscopy and a CCD detector.

Preparation of M-CS-MWNTs

For synthesis of M-CS-MWNTs NP hybrids first, 1.0 g of MWNTs was purified by refluxing at $80\text{ }^{\circ}\text{C}$ in concentrated HCl for 12 h, followed by filtration with a Millipore membrane (pore size $0.22\text{ }\mu\text{m}$) and a careful rinse with ultrapure water till the filtrate was neutral. Then, 1.0 g of purified MWNTs was refluxed in a mixed acid (concentrated $\text{H}_2\text{SO}_4 + \text{HNO}_3$, 75:25 vol%) at $80\text{ }^{\circ}\text{C}$ for 24 h [46]. The suspension was cooled and diluted with ultrapure water, followed by filtration and rinsing as above. The sample was dried in vacuum at $40\text{ }^{\circ}\text{C}$ for 24 h. For the synthesis of M-CS-MWNTs hybrids briefly, the obtained carboxylated MWNTs (40 mg) were sonicated in CS solution containing 5.0 cm^3 of 2.0 mg cm^{-3} CS in acetic acid solution and 0.4 g Fe_3O_4 for 20 min. The mixture was mechanically stirred for 16 h. A black product (M-CS-MWNTs) appeared and was separated from the reaction system by a magnet and washed for three times with ethanol and distilled water, respectively. Finally, M-CS-MWNTs were dried in an oven at 353 K under atmospheric condition. The product was subjected to thermogravimetric analysis to determine the degree of polymerization. The analysis of TGA data shows 18.8 % of polymeric chains are coated to the surface of MWNTs.

Adsorption of drug on functionalized MWNTs

In a typical experiment, about 50 mg of M-CS-MWNTs was incubated with 50 cm^3 of MTX solution (20 mg dm^{-3}).

Then it was placed to the thermostat shaker at 100 rpm and $25\text{ }^{\circ}\text{C}$. The initial pH of the MTX solutions was adjusted by adding 0.01 M HCl or NaOH. For different time interval, 5.0 cm^3 of dispersion was drawn and M-CS-MWNTs adsorbent was separated immediately by a magnet from treated solutions. Residual MTX concentration in the supernatant was obtained using a UV–Vis spectrophotometer at $\lambda_{\text{max}} = 372\text{ nm}$. Adsorbed amount of MTX per unit weight of dry M-CS-MWNTs at time t , and equilibrium [q_t and q_e (mg g^{-1})] and removal efficiency (η) of MTX were calculated by Eqs. (11)–(13), respectively:

$$q_t = \frac{C_0 - C_t}{m} V \quad (11)$$

$$q_e = \frac{C_0 - C_e}{m} V \quad (12)$$

$$\eta = \frac{C_0 - C_e}{C_0} \times 100\% \quad (13)$$

where C_0 , C_e , and C_t (mg dm^{-3}) are the MTX concentrations at initial, equilibrium, and time t , respectively, V (dm^3) is the solution volume and m (g) is the mass of nanocarrier used.

Drug loading optimization via full factorial design method

Full factorial design method, as a generic means of optimization, was applied to optimize the drug loading on M-CS-MWNTs through a decreased number of the experiments. Based on preliminary study of the effect of parameters on the drug loading, Minitab 16 software was applied for designing the experiment. Four variables at two levels: low and high were taken, which were represented by transforming values of -1 and $+1$, respectively. The values of these selected variables are shown in Table 1. Four parameters; pH, time, drug concentration, and M-CS-MWNTs dosage, were identified as key factors affecting the drug loading. The significance of the model and the regression coefficients were estimated by analysis of variance (ANOVA) combined with the application of Fisher's F test as well as Student T test at a probability P value of 0.05.

Acknowledgments The authors gratefully acknowledge the support of this work by the Imam Khomeini international university, Qazvin, Iran for financial support and providing laboratory facilities for this work.

References

1. Wong HL, Bendayan R, Rauth AM, Li Y, Wu XY (2007) Adv Drug Deliv Rev 59:491

2. Xiong XB, Ma ZS, Lai R, Lavasanifar A (2010) *Biomaterials* 31:757
3. Xu ZH, Zhang ZW, Chen Y, Chen LL, Lin LP, Li YP (2010) *Biomaterials* 31:916
4. Luo Y, Bernshaw NJ, Lu ZR, Kopecek J, Prestwich GD (2002) *Pharm Res* 19:396
5. Li XM, Ding LY, Xu YL, Wang YL, Ping QN (2009) *Int J Pharm* 373:116
6. Ishida T, Kirchmeier MJ, Moase EH, Zalipsky S, Allen TM (2001) *BBA Biomembranes* 1515:144
7. Mehnert W, Mader K (2001) *Adv Drug Deliv Rev* 47:165
8. Prabakaran M, Grailler JJ, Pilla S, Steeber DA, Gong SQ (2009) *Biomaterials* 30:6065
9. Iyer AK, Khaled G, Fang J, Maeda H (2006) *Drug Discov Today* 11:812
10. Kostarelos K, Lacerda L, Pastorin G, Wu W, Wiecekowsi S, Luangsivilay J, Godefroy S, Pantarotto D, Briand JP, Muller S, Prato M, Bianco A (2007) *Nat Nanotechnol* 2:108
11. Lacerda L, Russier J, Pastorin G, Herrero MA, Venturelli E, Dumortier H, Al-Jamal KT, Prato M, Kostarelos K, Bianco A (2012) *Biomaterials* 33:3334
12. Boncel S, Zajac P, Koziol KK (2013) *J Controlled Release* 169:126
13. Dhar S, Liu Z, Thomale J, Dai HJ, Lippard SJ (2008) *J Am Chem Soc* 130:11467
14. Feazell RP, Nakayama-Ratchford N, Dai H, Lippard SJ (2007) *J Am Chem Soc* 129:8438
15. Liu Z, Sun XM, Nakayama-Ratchford NH, Dai J (2007) *ACS Nano* 1:50
16. Pastorin G, Wu W, Wiecekowsi S, Briand JP, Kostarelos K, Prato M, Bianco A (2006) *Chem Commun* 11:1182
17. Kam NWS, Dai HJ (2005) *J Am Chem Soc* 127:6021
18. Kam NWS, Liu Z, Dai HJ (2005) *J Am Chem Soc* 127:12492
19. Ke G, Guan WC, Tang CY, Guan WJ, Zeng DL, Deng F (2007) *Biomacromolecules* 8:322
20. Chang PR, Zheng P, Liu B, Anderson DP, Yu J, Ma X (2011) *J Hazard Mater* 186:2144
21. Li C, Yang K, Zhang Y, Tang H, Yan F, Tan L, Xie Q, Yao S (2011) *Acta Biomater* 7:3070
22. Najeeb CK, Chang J, Lee JH, Lee M, Kim JH (2011) *J Colloid Interface Sci* 354:461
23. Fagnoni M, Profumo A, Merli D, Dondi D, Mustarelli P, Quaratarone E (2009) *Adv Mater* 21:1761
24. Rungrotmongkol T, Arsawang U, Iamsamai C, Vongachariya A, Dubas ST, Ruktanonchai U, Soottitantawat A, Hannongbua S (2011) *Chem Phys Lett* 507:134
25. Sangsanoh P, Supaphol P (2006) *Biomacromolecules* 7:2710
26. Yu Z, Brus LE (2000) *J Phys Chem* 104:10995
27. Xu D, Hein S, Wang K (2008) *Mater Sci Technol* 24:1076
28. Guibal E (2004) *Sep Purif Technol* 38:43
29. Iamsamai C, Hannongbua S, Ruktanonchai U, Soottitantawat A, Dubas ST (2010) *Carbon* 48:25
30. Modi CD, Patel SJ, Desai AB, Murthy R (2011) *J Appl Pharm Sci* 1:103
31. Prato M, Kostarelos K, Bianco A (2008) *Acc Chem Res* 41:60
32. Chen M, He Y, Chen X, Wang J (2012) *Langmuir* 28:16469
33. Yang D, Yang F, Hu JH, Long J, Wang CC, Fu DL, Ni QX (2009) *Chem Commun* 13:4447
34. Dyke A, Tour JM (2003) *J Am Chem Soc* 125:1156
35. Marroquin J, Kim HJ, Jung DH, Rhee KY (2012) *Carbon Lett* 13:126
36. Rhim J, Hong S, Park H, Ng PKW (2006) *J Agric Food Chem* 54:5814
37. Yang SB, Shao DD, Wang XK, Nagatsu M (2014) *RSC Adv* 4:4856
38. Yang SB, Hu J, Chen CL, Shao DD, Wang XK (2011) *Environ Sci Technol* 45:3621
39. Dash S, Murthy PN, Nath L, Chowdhury P (2010) *Drug Res* 67:217
40. Cheung WH, Szeto YS, McKay G (2007) *Bioresour Technol* 98:2897
41. Ma W, Ya FQ, Han M, Wang R (2007) *J Hazard Mater* 143:296
42. Kumar KV (2006) *J Hazard Mater B* 137:1538
43. Ho YS (2006) *Water Res* 40:119
44. Khaled A, Nemr AE, Sikaily AE, Abdelwahab O (2009) *J Hazard Mater* 165:100
45. Venkatesha TG, Viswanatha R, Nayaka YA, Chethana BK (2012) *Chem Eng J* 198:1
46. Datsyuk V, Kalyva M, Papagelis K, Parthenios J, Tasisb D, Siokou A, Kallitsis I, Galiotis C (2008) *Carbon* 46:833
47. Mahumder A, Goyal A (2008) *Bioresour Technol* 99:3685
48. Hou XJ, Chen W (2008) *Carbohydr Polym* 72:67
49. Garcia-Munoz RA, Morales V, Linares M, Gonzalez PE, Sanz R, Serrano DP (2014) *J Mater Chem B* 2:7996
50. Bingol D, Tekin N, Alkan M (2010) *Appl Clay Sci* 50:315